Direct and Indirect Electron Emission from the Green Fluorescent Protein Chromophore

Y. Toker, D. B. Rahbek, B. Klærke, A. V. Bochenkova, and L. H. Andersen
Department of Physics and Astronomy, Aarhus University, DK-8000 Aarhus C, Denmark
(Received 30 April 2012; published 18 September 2012)

Photoelectron spectra of the deprotonated green fluorescent protein chromophore have been measured in the gas phase at several wavelengths within and beyond the S_0-S_1 photoabsorption band of the molecule. The vertical detachment energy (VDE) was determined to be 2.68 ± 0.1 eV. The data show that the first electronically excited state is bound in the Franck-Condon region, and that electron emission proceeds through an indirect (resonant) electron-emission channel within the corresponding absorption band.

DOI: 10.1103/PhysRevLett.109.128101 PACS numbers: 87.64.ks, 33.80.Eh

The green fluorescent protein (GFP) is extensively used as a marker in biology owing to its remarkable fluorescent properties [1]. The photoactive molecular unit (chromophore) in wild-type GFP is *p*-hydroxybenzylideneimidazolinone (*para*-HBDI)—see Fig. 1. The chromophore is strongly fluorescent while being inside the barrel-shaped protein which keeps the chromophore in a planar configuration by a network of hydrogen bonds. When the chromophore is in vacuum, the dominant deexcitation pathways are internal conversion through nuclear rearrangement and electron emission [2,3].

Studies of the isolated chromophore provide a helpful reference for understanding the important, but complicated interplay between the protein and its chromophore molecule. The first experimental gas-phase absorption measurement with a deprotonated *para*-HBDI chromophore was reported over ten years ago [2]. Later this measurement was repeated in other laboratories [3–5], and also studied theoretically [6–8]. Based on action spectroscopy, where the action in turn was based on internal conversion and statistical fragmentation, the measurements show a maximum fragmentation yield at ~480 nm which coincides with the absorption maximum of the entire protein and hence gives indications of rather ''gentle'' interactions inside the chromophore pocket in GFP. Indeed, some of the protein properties like the fluorescence color, can be controlled by modifications of the active chromophore emphasizing the importance of the isolated chromophore properties [9].

For understanding the dynamics of the *para*-HBDI chromophore upon photoexcitation its vertical detachment energy (VDE) must be determined. In contrast to normal absorption spectroscopy, electron detection allows the energy levels to be determined relative to the electronic continuum. This provides an additional test of molecular-quantum theory, and gives a vacuum reference for GFP proteins. Correspondingly, our group as well as others [10,11] have simultaneously measured and characterized the photoelectrons from the deprotonated GFP chromophore in vacuum (experimentally, electron emission was previously inferred indirectly through loss of parent ions that did not lead to charged fragments upon photoexcitation [4]). Here, in addition to measuring the VDE, we study the competition between the different deexcitation pathways leading to electron emission by measuring the photoelectron spectra at several wavelengths within and beyond the first photoabsorption band. The results reveal a competition between direct and indirect electron emission, as explained below, which are alternative ''action''routes to internal conversion—see Fig. 2.

The experimental setup has been described in detail [12]; however, several modifications were made to facilitate detection of low energy electrons from biomolecules and to achieve better resolution. The setup consists of an electrospray ion source, which includes a multipole trap for ion accumulation. At a rate of 10 Hz, ions were extracted from the ion source and accelerated to a kinetic energy of 20 keV. The ions were then mass-selected using a magnet and steered into the interaction region where the ions were irradiated by a nanosecond laser pulse. The laser used in this work is an EKSPLA tunable optical parametric oscillator laser, which was operated at 20 Hz. Half of the laser shots, in which ions were not present, were used for background subtraction. Electrons produced in the interaction region were accelerated by an electric field towards a microchannel plate (MCP) detector (labeled E-MCP in Fig. 3), where their position and time of flight were recorded. The main ion beam as well as neutral fragments continued and passed through a hole in the center of the E-MCP detector. A deflector was used 0.45 m downstream to steer away the main ion beam, while the neutral fragments were counted by a second MCP detector (labeled N-MCP in Fig. 3). Thus, in the process of photoemission from negative ions, $A^- + \hbar\omega \rightarrow A + e^-$, the position and

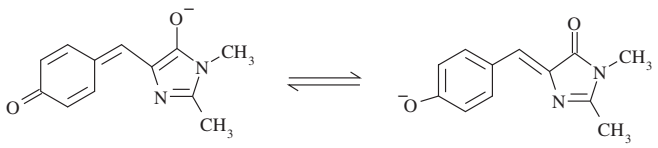

FIG. 1. The two resonance forms of the deprotonated GFP model chromophore *para*-HBDI ion.

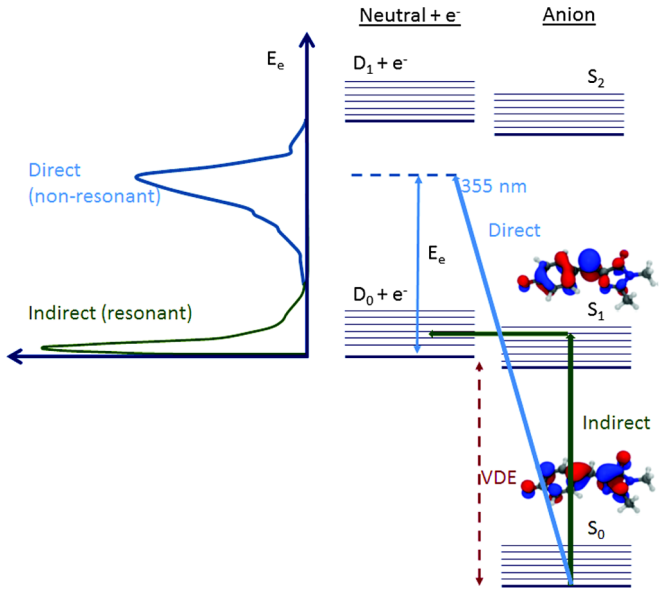

FIG. 2 (color online). Direct and indirect electron emission shown schematically. S_0 is the electronic ground state and S_1 is the first electronically excited state of the anion. D_0 is the ground state of the neutral chromophore.

time of flight of both the electron and neutral molecule A were measured.

The interaction region, whose total length is 275 mm, consists of 25 equally spaced electrodes. The interaction point between the laser light and the ions is centered between the 7th and 8th electrode. The potentials applied to the electrodes are shown in Fig. 3, and consist of a linearly decreasing potential between electrodes 1 and 10, and a steeper potential slope between electrodes 11 and 25. The change in slope produces electrostatic focusing, and the voltages were adjusted such that the detector was at the focal plane. Thus, velocity map imaging conditions are achieved; i.e., the final position of the electron does not depend on the point of birth but only on the velocity in the plane perpendicular to the ion beam. We denote the ion beam axis as the z direction, and the perpendicular plane as the x, y plane. The position of hits on the detector depends only on the initial v_x, v_y components of the electron velocity.

Photodetachment from *para*-HBDI results in very low energy electrons which under normal operating conditions would continue colinearly with the ion beam and exit the spectrometer region through the hole in the center of the detector. Therefore a small magnetic field of $B = 0.6$ Gauss was introduced, causing the electrons to be slightly deflected from the central ion-beam axis and hit the detector off axis. We denote the direction of the electric field as the z axis. For a small magnetic field one can neglect the effect of the field on the motion along the z axis, which is determined by the classical equation: $\ddot{z} = \frac{q}{m}E$, where q and m are the electron charge and mass, respectively, and E is

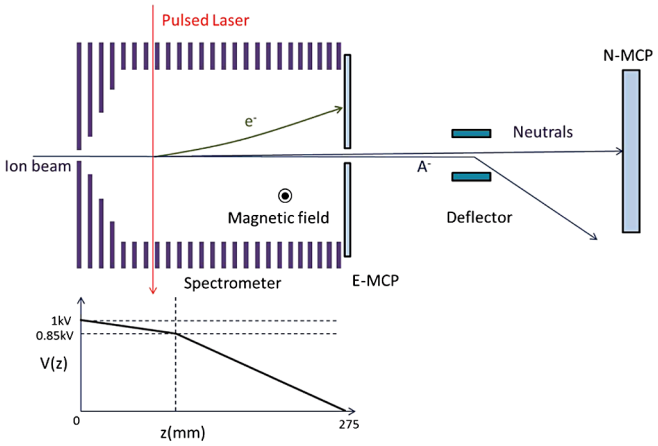

FIG. 3 (color online). Schematic illustration of the interaction region and the positions of detectors in the experiment.

the electric field. Denoting x as the axis perpendicular to both $\hat{z}$ and $\vec{B}$, the displacement along this axis can be determined by integrating $\ddot{x} = -\frac{q}{m}B_y\dot{z}$ to yield

$$x = -\frac{q^2 B_y E}{6m^2}t^3 = -\sqrt{\frac{2qL^3}{9m}}\frac{B_y}{\sqrt{E}}. \quad (1)$$

Here, B_y is the component of the magnetic field in the perpendicular direction to the z axis, t is the time of flight towards the detector, and L is the distance between the interaction point and the detector. Thus, the displacement is linear with magnetic field, but is inversely proportional to the square root of the electric field. This agrees well with numerical simulations. Electron trajectories were calculated with the SIMION [13] simulation program with the applied potential profile. The same voltage settings which provide focusing when no magnetic field is present, also provide focusing in the presence of the magnetic field, and it was verified that the final position of the electrons on the screen was independent of the point of birth, linear with the initial velocity in the x, y direction, and that the linearity coefficient is the same in both directions. The setup was calibrated by measuring the photoelectron spectrum of an O^- beam, produced in a cold plasma ion source and irradiated by $\lambda = 600$ nm laser pulses. For the production of chromophore ions, the ion source was switched to the electrospray-ion source and photoelectron spectra were measured for several representative wavelengths within and beyond the chromophores absorption band.

Figure 4 (left) shows the position distribution of the hits on E-MCP. As opposed to the case of photoemission from atomic anions, no sharp circles are visible, rather the data, here recorded at 500 nm, suggests that the electrons are released with a broad distribution of low energies. In addition no angular dependence was observed. Figure 4 (right) shows the corresponding radial distribution. After one step of smoothing a Monte Carlo algorithm was used to produce

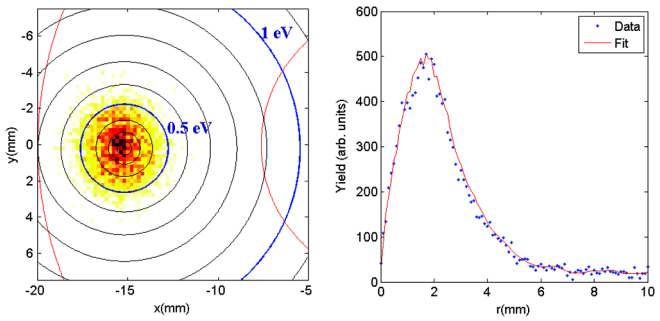

FIG. 4 (color online). Left: Image of electron hits on the E-MCP detector, for *para*-HBDI irradiated at $\lambda = 500$ nm. The lines centered around (0,0) indicate the boundaries of the detector. Right: The radial distribution of the data.

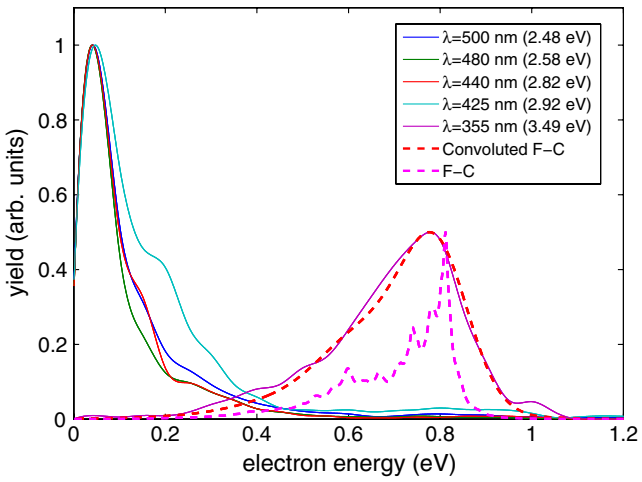

FIG. 5 (color online). Photoelectron-energy distribution for *para*-HBDI. Shown are experimental data obtained at a series of wavelengths and the calculated distribution convoluted by an experimental energy resolution function at 355 nm. Also shown is the nonconvoluted Franck-Condon (F-C) distribution at 300 K.

an electron-energy distribution which fits the measured radial distribution, shown as the red line in Fig. 4 (right).

Figure 5 presents the obtained electron-energy distributions for a range of different wavelengths. At low photon energy, the data consist of a low-energy peak, centered at ~0.05 eV whose shape essentially does not change with wavelength. Although most electrons are produced with low energy, the peak has a tail extending up to 0.3 eV which corresponds to the average thermal energy within the molecule as calculated from its vibrational frequencies. These low energy electrons could be a result of electron emission from the S_1 state through the process

$$\hbar\omega + S_0(v) \rightarrow S_1(v') \rightarrow D_0(v'') + e^-, \qquad (2)$$

which we here denote as ''indirect'' (or resonant) electron emission. Alternatively, they could result from thermionic emission, in which, following internal conversion, electrons are emitted from the hot ground state, a process which Verlet [10] indicates as more likely. Nevertheless, in the case of thermionic emission the energy of the emitted electrons should depend on the wavelength of the exciting laser. Moreover, the time scale for thermionic emission is very long—on the tens of microsecond time scale [2,14,15]. We see no evidence of delayed electron emission and conclude that the low-energy peak in the spectrum is a result of indirect electron emission.

With increasing photon energy the resonant $S_0 \rightarrow S_1$ absorption decreases and a high-energy peak appears in the electron spectrum which corresponds to direct (nonresonant) electron emission:

$$\hbar\omega + S_0(v) \rightarrow D_0(v') + e^-. \qquad (3)$$

At 355 nm indirect electron emission is no longer seen since the excitation is not resonant with any electronically excited anion states (Fig. 2).

The width of the nonresonant peak in the photoelectron spectrum is determined by the vibrational structure of the $S_0 \rightarrow D_0 + e^-$ electronic transition. The Frank-Condon envelope takes into account the initial vibrational levels of the anions which are populated at room temperature as well as the many accessible vibrational levels of the neutral. The Frank-Condon envelope of the S_0 to D_0 transition was calculated using a time-domain formalism based on Fourier transforms of Lax's autocorrelation function within the double harmonic parallel-mode approximation [16]. Geometry parameters and vibrational frequencies in the ground electronic states of the anion and neutral radical were found using the PBE0/(aug)-cc-pVDZ functional in the frame of the Firefly quantum chemistry package [17]. As the Frank-Condon envelope only determines the shape of the electron energy distribution and not the absolute position in energy, the calculated curve was shifted to match the experimental data. Indeed good correspondence between experiment and theory can be made. The resulting VDE is determined to be 2.68 ± 0.1 eV, 0.04 eV lower than obtained from the peak position of the experimental data in Fig. 5. This value is slightly lower than the recently reported value of 2.85 ± 0.1 eV [11] and 2.8 ± 0.1 eV [10], but within the combined error bars.

The experimental data are close to but slightly higher than the recently reported VDE of 2.5 eV (corresponding to $\lambda = 496$ nm) [8]. Importantly, it was suggested that the S_1 state is unbound since the VDE was below the calculated vertical excitation energy (VEE) of 2.6 eV [8]. XMCQDPT2 [18] calculations by our group [15] give a VDE of 2.62 eV and a VEE of 2.52 eV suggesting that the S_1 state is bound. The present experimental results also suggest that S_1 is bound in the Franck-Condon region. The kinetic energy of the photoelectrons, monitored as a function of excitation wavelengths, reveals a nearly constant narrow energy distribution peaked at very low energy (0.05 eV) for a wide range of photon energies (2.48 − 2.82 eV). In other words, in this photon-energy region

the electron energy does not shift with the wavelength as in the classical photoelectric effect. Moreover, all experimentally determined values of the VDE are higher than the peak position in the action photoabsorption spectra (2.57 eV) [2,3]. The existence of a competing internal conversion channel [2,3] gives further support for assigning the S_1 state as electronically bound.

Electron emission is observed to occur even below the VDE, through indirect electron emission. Here, energy is being transferred from the nuclear to the electronic degrees of freedom, a process known as vibrational autodetachment [19]. Interestingly, the VDE of 2.68 eV ($\sim$ 460 nm) coincides with the photon energy beyond which internal conversion almost ceases to occur [2,3,15]. Thus above the VDE the direct electron emission channel opens while internal conversion is suppressed. Nevertheless, within the visible absorption band *indirect* electron emission is dominant. At 425 nm, for example, the majority of electrons are produced with $\sim$0.05 eV, through the indirect channel, and the contribution from direct electron emission, resulting in a shoulder of higher energy electrons is apparent, but small. Finally, beyond the absorption band direct electron emission becomes the only and therefore the dominant reaction pathway.

Identifying the different electron emission channels opens interesting questions regarding the dynamics of the outgoing electron. The threshold behavior of the detachment process was discussed many years ago by Wigner [20] who pointed out the generalities that apply, and O'Malley extended the theory to include long-range multipole forces [21]. These corrections are of particular importance when dealing with a complex polar molecule like the HBDI. The electron emission process involves a final-state interaction with a centrifugal barrier $V_c \propto \frac{l(l+1)}{r^2}$, l being the angular momentum of the outgoing electron, as well as a charge-dipole interaction of the form $V_d \propto -\frac{d}{r^2}$ where d is the dipole moment of the neutral radical chromophore. The relative strength between the two terms determines the actual threshold behavior [21], and in the limit where $d = 0$, the Wigner form $\sigma \sim k^{2l+1}$ applies [20]. When d becomes greater than $(l + 1/2)$, solutions emerge where the cross section does not vanish at threshold, but rather oscillates with constant amplitude and increasing frequency as the threshold is approached [21]. The dipole moment of the neutral radical chromophore was indeed estimated to be very large, 7 Debye (2.75 a.u.) [15].

In summary, we identified direct (nonresonant) $S_0 \rightarrow D_0 + e^-$ as well as indirect resonant $S_0 \rightarrow S_1 \rightarrow D_0 + e^-$ electron emission channels in the photoelectron spectra of the *para*-HBDI GFP chromophore in the gas phase. In a spectral region with no resonant contribution we measured the vertical detachment energy to be 2.68 eV $\pm$ 0.1 eV. The shape of the nonresonant part of the spectrum was found to be well reproduced by the calculated Franc-Condon overlap between the involved electronic states. Importantly, the first electronic excited state is found to be bound.

We are thankful to Xavier Urbain for the idea of using a small magnetic field for deflecting the electrons of the main axis. This work is supported by the Lundbeck Foundation, the Carlsberg Foundation, the Danish Research Agency and the Marie Curie European Career Integration Grant within the 7th European Community Framework Programme. A. V. B. acknowledges support from the RFBR (Grant No. 11-03-01214).

[1] R. Y. Tsien, Annu. Rev. Biochem. **67**, 509 (1998).
[2] S. B. Nielsen, A. Lapierre, J. U. Andersen, U. V. Pedersen, S. Tomita, and L. H. Andersen, Phys. Rev. Lett. **87**, 228102 (2001).
[3] M. W. Forbes and R. A. Jockusch, J. Am. Chem. Soc. **131**, 17038 (2009).
[4] M. W. Forbes, A. M. Nagy, and R. A. Jockusch, Int. J. Mass Spectrom. **308**, 155 (2011).
[5] T. Tanabe, M. Saito, and K. Noda, Eur. Phys. J. D **62**, 191 (2011).
[6] S. Wan, S. Liu, G. Zhao, M. Chen, K. Han, and M. Sun, Biophys. Chem. **129**, 218 (2007).
[7] L. H. Andersen and A. V. Bochenkova, Eur. Phys. J. D **51**, 5 (2009).
[8] I. V. Polyakov, B. L. Grigorenko, E. M. Epifanovsky, A. I. Krylov, and A. V. Nemukhin, J. Chem. Theory Comput. **6**, 2377 (2010).
[9] R. N. Day and M. W. Davidson, Chem. Soc. Rev. **38**, 2887 (2009).
[10] D. A. Horke and J. R. R. Verlet, Phys. Chem. Chem. Phys. **14**, 8511 (2012).
[11] C. Mooney, M. E. Sanz, A. R. McKay, R. J. Fitzmaurice, A. E. Aliev, S. Caddick, and H. H. Fielding, J. Phys. Chem. A **116**, 7943 (2012).
[12] H. B. Pedersen, M. J. Jensen, C. P. Safvan, X. Urbain, and L. H. Andersen, Rev. Sci. Instrum. **70**, 3289 (1999).
[13] I. source software, Simion, version 8, http://simion.com.
[14] J. U. Andersen, E. Bonderup, and K. Hansen, J. Phys. B **35**, R1 (2002).
[15] A. V. Bochenkova, J. Rajput, D. Rahbek, B. Klærke, and L. H. Andersen, Nat. Chem. (to be published).
[16] P. V. Yurenev, M. K. Kretov, A. V. Scherbinin, and N. F. Stepanov, J. Phys. Chem. A **114**, 12804 (2010).
[17] A. A. Granovsky, Firefly, version 7.1.G., http://classic.chem.msu.su/gran/firefly/index.html.
[18] A. A. Granovsky, J. Chem. Phys. **134**, 214113 (2011).
[19] J. Simons, J. Phys. Chem. A **112**, 6401 (2008).
[20] E. P. Wigner, Phys. Rev. **73**, 1002 (1948).
[21] T. F. O'Malley, Phys. Rev. **137**, A1668 (1965).